ORIGINAL ARTÍCULO

View factor calculations between triangular surfaces

Cálculo del factor de visión entre superficies triangulares

Yanan Camaraza-Medina[1*]

[1]University of Guanajuato, Guanajuato, México.

[*]Autor para la correspondencia: ycamaraza1980@gmail.com

Abstract

The view factor between surfaces is of paramount importance in the assessment of radiant energy exchange. Nowadays the available technical literature lacks the analytical expression for estimating the vision factor for combining triangular surfaces. An analytical solution requires the addition of multiple integrals, due to the changes in the integration contours, which becomes more complex for irregular contours. This research aims to develop an expression to calculate the view factor between 32 triangular geometric configurations with common edge and included angle θ. To establish comparisons, 48 cases with various geometric relationships were calculated, using analytical solution (AS), numerical integration by means of Simpson's rule 1/3 (SMR), Sauer's graphical solution (SGS) and Bretzhtsov's cross roots (BCR). From eight basic geometries, the vision factor for the remaining 24 combinations was calculated using the addition rule. In all cases, identical fit values of RMS and SGS respect to AS were obtained, while RCB showed the best correlation in all cases examined. The results of this research revel that the proposal constitutes a suitable tool to be used in thermal engineering given the practical nature of the contribution and reasonable values of obtained fits.

Keywords: view factor, Bretzhtsov's cross-root, radiative heat transfer, triangular surfaces

Resumen

En la evaluación del intercambio de energía radiante el factor de visión entre superficies es de vital importancia. Actualmente la literatura técnica disponible carece de una expresión analítica para estimar el factor de visión para combinaciones de superficies triangulares. Una solución analítica requiere la suma de múltiples integrales, dados los cambios en los contornos de integración, lo que se complejiza en contornos irregulares. Este trabajo tuvo como objetivo desarrollar una expresión para computar el factor de visión entre 32 configuraciones geométricas triangulares con arista común y ángulo incluido θ. Para establecer comparaciones, se calcularon 48 casos con

diversas relaciones geométricas, utilizando la solución analítica (SA), la integración numérica mediante la regla múltiple de Simpson 1/3 (RMS), la solución gráfica de Sauer (SGS) y las raíces cruzadas de Bretzhtsov (RCB). A partir de ocho geometrías básicas, se computó el factor de visión para las restantes 24 combinaciones mediante la regla de la suma. En todos los casos, se obtuvieron valores de ajuste idénticos de RMS y SGS con respecto a AS, mientras que la RCB mostró la mejor correlación en todos los casos examinados. Dada la naturaleza práctica de la contribución y los valores razonables de los ajustes obtenidos, la propuesta constituye una herramienta adecuada para su aplicación en ingeniería térmica.

Palabras clave: factor de visión, raíz cruzada de Bretzhtsov, transferencia de calor por radiación, superficies triangulares

1. INTRODUCTION

In many engineering applications, it is necessary to evaluate radiative heat transfer between surfaces. The view factor allows for the calculation of the fraction of radiant energy emitted by one surface that reaches another. Consequently, the geometric relationship between two surfaces and its influence on the view factor has been a subject of research for decades. Previous works have proposed various analytical and numerical solutions for different configurations (Howell and Mengüç, 2011; Nassar, 2020; Modest and Mazumder, 2021; Camaraza-Medina, 2021; Camaraza-Medina et al., 2022). An extensive compilation of view factors for over 340 different configurations is provided by Howell (2023).

Several methods are known in specialized literature for estimating view factors, including graphical, analytical, and visual approaches. Furthermore, by employing summation rules and algebraic factors, view factors for known geometries can be utilized to determine those of derived or more complex geometries (Narayanaswamy, 2015; Narayanaswamy and Meyappan, 2015; Gupta et al., 2017; Howell et al., 2020).

The current increase in data processing capabilities within computational techniques has enabled the use of commercial software based on the Finite Element Method (FEM) to solve various heat transfer problems, including thermal radiation. Solutions for edge and boundary problems generally reduce to surfaces with a common edge and an included angle θ, for which analytical solutions are already known (Ehlert and Smith, 1993; Yi et al., 2019; Zhou et al., 2020; Reddy et al., 2023). However, in modern engineering, mesh generators rarely utilize rectangles or squares (unless the global geometry is a perfect cube), with triangular elements being the most widely used.

The analytical solution (AS) for the view factor between triangular geometries requires the summation of multiple integrals due to changes in integration contours, which hinders the derivation of solutions for complex configurations. Numerical integration may offer a partial solution to the problem; however, specialized literature contains few contributions to this specific topic (Krishnaprakas, 1997).

Using numerical integration via Simpson's 1/3 rule (SMR) with five intervals, view factors were obtained for various triangular geometries with a common edge and an angle θ=90°, plotting the results for the most elementary cases and deriving the remaining geometries through the use of summation rules (Sauer, 1974). Sauer's graphical solutions (SGS) are useful but require the interpretation of graphs, which introduces reading and interpretation errors; therefore, they are unsuitable for triangular mesh generation and subsequent view factor calculation, as they lack an analytical solution or numerical approximation for their estimation.

The Bretzhtsov cross-root (BCR) method is a mathematical tool that allows for reasonable adjustments in approximations of complex functionals, in addition to generating an analytical expression that includes the boundary conditions or unknowns to be treated; thus, it can be utilized for view factor calculations without the need for graphs or their interpretation. The method in question allows for piecewise or branch-wise fitting, with common nodes for several solutions (Camaraza-Medina et al., 2022). Its mathematical conception is similar to that of the FEM, making it suitable for this work.

Currently, specialized literature does not provide an analytical expression to directly calculate the view factor for combinations of triangular surfaces. In the expanded compilation of available view factor configurations, it is verified that only Sauer's graphical results are used for the case of finite triangular surfaces (Howell, 2023). Other consulted sources also present Sauer's graphs for the determination of view factors (Thyageswaran, 2022; Camaraza-Medina, 2023). This demonstrates that exact or approximate analytical solutions for determining view factors between triangular geometries with a common edge and an included angle θ do not currently exist, which constitutes the main objective of this work.

Therefore, this research intends to develop approximate solutions that allow for computing the view factor in various triangular geometries, which do not present high mathematical complexity and whose correlation with respect to the AS offers a better fit than the SGS, thus constituting a new analysis method for application to view factor calculation via FEM, in addition to establishing new expressions that can be included in existing catalogs.

This paper presents exact analytical solutions for eight basic triangular geometries and their respective BCRs. To establish comparisons, 48 examples with various aspect ratios were calculated for each geometry, using the analytical solution, the numerical solution of the quadruple integral via SMR with five intervals, Sauer's graphical solution, and the view factors calculated using Bretzhtsov's cross-roots (BCR). From the eight basic geometries, the view factor for another 24 triangular geometries is obtained using summation rules. In all cases, identical fit values for SMR and SGS with respect to the AS were obtained, while the BCR showed the best fit in all examined cases, confirming the validity of the hypothesis regarding its use.

Given the practical nature of the contribution and the reasonable values of the fits obtained, the proposal constitutes a suitable tool for application in thermal engineering and related practices requiring thermal radiation calculations.

2. METHODOLOGY

2.1 Basic Considerations on the View Factor

The view factor is fundamental to the exchange of radiant energy. It depends on the configuration and position of the receiving and emitting surfaces, making its evaluation complex and, in many cases, prone to erroneous results. Thus, the view factor F_{12} is the fraction of radiation emitted by surface A_1 that is intercepted by surface A_2, expressed as Equation (1), according to Boeke and Wall (1976):

$$F_{12} = \frac{1}{\pi A_1} \int_{A_1}^{A_2} \int_{A_2}^{A_1} \frac{\cos\theta_1 \cos\theta_2}{r^2} \, dA_1 \, dA_2 \tag{1}$$

where: A_1, A_2 are the emitting and receiving surfaces, respectively. θ_1, θ_2 are the angles between the normal vector to area dA_1, dA_2 and the line joining the center of surfaces A_1, A_2 ; respectively. r is the distance between the centers of surfaces A_1 y A_2, (Figure 1).

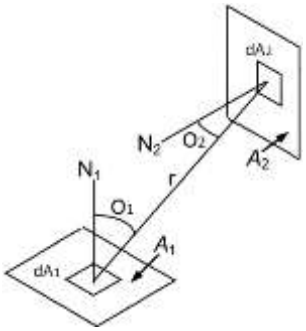

Figure 1. Basic geometry for the definition of the view factor.

Equation (1) involves double integration, which can be a very laborious mathematical problem in many instances. Therefore, calculating the view factor for any geometry requires handling a considerable volume of integrals and solving complex mathematical equations. To simplify the analysis, numerical approximations providing adequate fits with a reasonable margin of error are used, allowing for their application in practical engineering. For three-dimensional configurations, various methods can be implemented to estimate the view factor, such as direct integration, contour integration, summation and reciprocity techniques, SMR, Monte Carlo method, ray tracing, FEM, and matrix methods (Francisco et al., 2014; Bonnici et al., 2019; Sönmez et al., 2019; Lakhi and Safavinejad, 2021; Biehs et al., 2021; Camaraza-Medina et al., 2023).

In this research, to obtain the view factors associated with the 32 studied configurations, the direct integration method was implemented; and the BCR method was used to approximate the special functions generated in the direct integration.

2.2. Mathematical Solution of the View Factor

The view factor between two finite rectangles of the same width with a common edge and included angle θ (Figure 2) is given by (2):

$$f_{(1)} = F_{a-b} = \frac{1}{\pi A_1}\iint \frac{\cos O_1 \cos O_2 \, dA_1 dA_2}{r^2} = \frac{\sin^2\theta}{\pi A_1}\int_0^L dy_1 \int_0^D dx \int_0^w dz \int_0^D \frac{xz}{\{(y_1-y_2)^2+x^2+z^2-2xz\cos\theta\}^2} dy_2 \qquad (2)$$

To evaluate Equation (2), the following definitions expressed in (3) are used:

$$X = W/D \quad ; \quad Y = L/D \quad ; \quad R = \sqrt{X^2 + Y^2 - 2XY\cos\theta} \qquad (3)$$

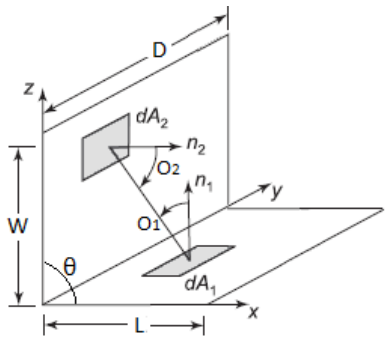

Figure 2. Rectangles with common edge and included angle θ

Evaluating Equation (2), the following solution is obtained (Hamilton and Morgan, 1952), expressed in (4):

$$f_{(1)} = \mathrm{F_{a-b}} = \frac{1}{\pi Y}\left\{\begin{array}{c} -\frac{\sin 2\theta}{4}\left\{Y^2\tan^{-1}\left(\frac{X}{Y}\csc\theta-\cot\theta\right)+X^2\tan^{-1}\left(\frac{Y}{X}\csc\theta-\cot\theta\right)+XY\sin\theta+\left(\frac{\pi}{2}-\theta\right)(X^2+Y^2)\right\}+ \\ +\frac{1}{4}\ln\left\{\left\{\frac{X^2}{R^2}\left(\frac{1+X^2}{1+R^2}\right)^{\cos 2\theta}\right\}^{X^2\sin^2\theta}\left(\frac{Y^2+Y^2R^2}{R^2+Y^2R^2}\right)^{Y^2\sin^2\theta}\left(\frac{(1+X^2)(1+Y^2)}{1+R^2}\right)^{\cos^2\theta+1}\right\}+ \\ +(\sin^3\theta\cos\theta)\tan^{-1}\left(\frac{Y\sin\theta\sqrt{X^2+\cot^2\theta+1}}{X^2-YX\cos\theta+1}\right)\sqrt{X^4+X^2(\cot^2\theta+1)}++X\tan^{-1}\left(\frac{1}{X}\right)+ \\ +Y\tan^{-1}\left(\frac{1}{Y}\right)+-R\cot^{-1}(R)+\frac{\sin 2\theta}{2}\int_0^Y\sqrt{z^2+\cot^2\theta+1}\tan^{-1}\left(\frac{X\sin\theta\sqrt{z^2+\cot^2\theta+1}}{z^2-zX\cos\theta+1}\right)dz \end{array}\right\} \quad (4)$$

In Equations (2) and (4), the angle θ is given in radians.

In a previous investigation (Hamilton and Morgan, 1952), an expression similar to Equation (4) was obtained to solve the quadruple integral given in Equation (2), tabulating view factor values for angles tabulando los valores de los factores de visión para los ángulos $\theta = (30°; 45°; 60°; 90°; 120°; 135°; 150°)$. These values were subsequently corrected for failing to comply with summation rules in some cases (Feingold, 1966; DeSutter et al., 2019; Yarahmadi et al., 2020; Thyageswaran, 2022; Camaraza-Medina, 2023).

Equation (4) is highly complex. The final integral lacks primitives, making it impossible to solve analytically; thus, its solution will be obtained via SMR (with eight intervals). In each numerical integration interval, the variable z is replaced by its corresponding fraction of the emitting surface length L (Table 1), obtaining a solution (ω_n) for each interval (Thyageswaran, 2022).

Table 1. Definition of z values for SMR, Equation (4)

0	Interv. 1	Interv. 2	Interv. 3	Interv. 4	Interv. 5	Interv. 6	Interv. 7	Interv. 8
0	$0{,}125L$	$0{,}25L$	$0{,}375L$	$0{,}5L$	$0{,}625L$	$0{,}75L$	$0{,}875L$	L
ω_1	ω_2	ω_3	ω_4	ω_5	ω_6	ω_7	ω_8	ω_9

Therefore, the numerical evaluation of the last integral given in Equation (4) can be calculated as shown in (5):

$$\int_0^Y \left\{\sqrt{1+z^2\sin^2\theta}\,\tan^{-1}\left(\frac{X\sqrt{1+z^2\sin^2\theta}}{z^2-zX\cos\theta+1}\right)\right\}dz$$

$$\cong \frac{L}{24}\left(\omega_1+\omega_9+2(\omega_3+\omega_5+\omega_7)+4(\omega_2+\omega_4+\omega_6+\omega_8)\right) \quad (5)$$

If $\theta = 90^{\circ}$,holds, then Equation (4) simplifies to the following relationship, given in (6):

$$f_{(1)} = F_{a-b} = \frac{1}{\pi Y}\left\{X\tan^{-1}\left(\frac{1}{X}\right)+Y\tan^{-1}\left(\frac{1}{Y}\right)-R\cot^{-1}(R)+\right.$$
$$\left.\frac{1}{4}\ln\left\{\left(\frac{X^2+X^2R^2}{R^2+X^2R^2}\right)^{X^2}\left(\frac{Y^2+Y^2R^2}{R^2+Y^2R^2}\right)^{Y^2}\left(\frac{(1+X^2)(1+Y^2)}{1+R^2}\right)\right\}\right\} \quad (6)$$

In Equation (6), the following definitions given in (7) are utilized:

$$X = W/D \quad ; \quad Y = L/D \quad ; \quad R = \sqrt{X^2+Y^2} \quad (7)$$

Figure 3 graphically presents the solutions of Equation (4) for values of $\theta = \left(30^{\circ}, 45^{\circ}, 60^{\circ}, 90^{\circ}, 120^{\circ}, 150^{\circ}\right)$,, in the intervals $0.1 \leq Y \leq 10$ y $0.1 \leq X \leq 10$. For angle values $\theta \neq \left(30^{\circ}, 45^{\circ}, 60^{\circ}, 90^{\circ}, 120^{\circ}, 150^{\circ}\right)$, the view factor can be obtained via interpolation.

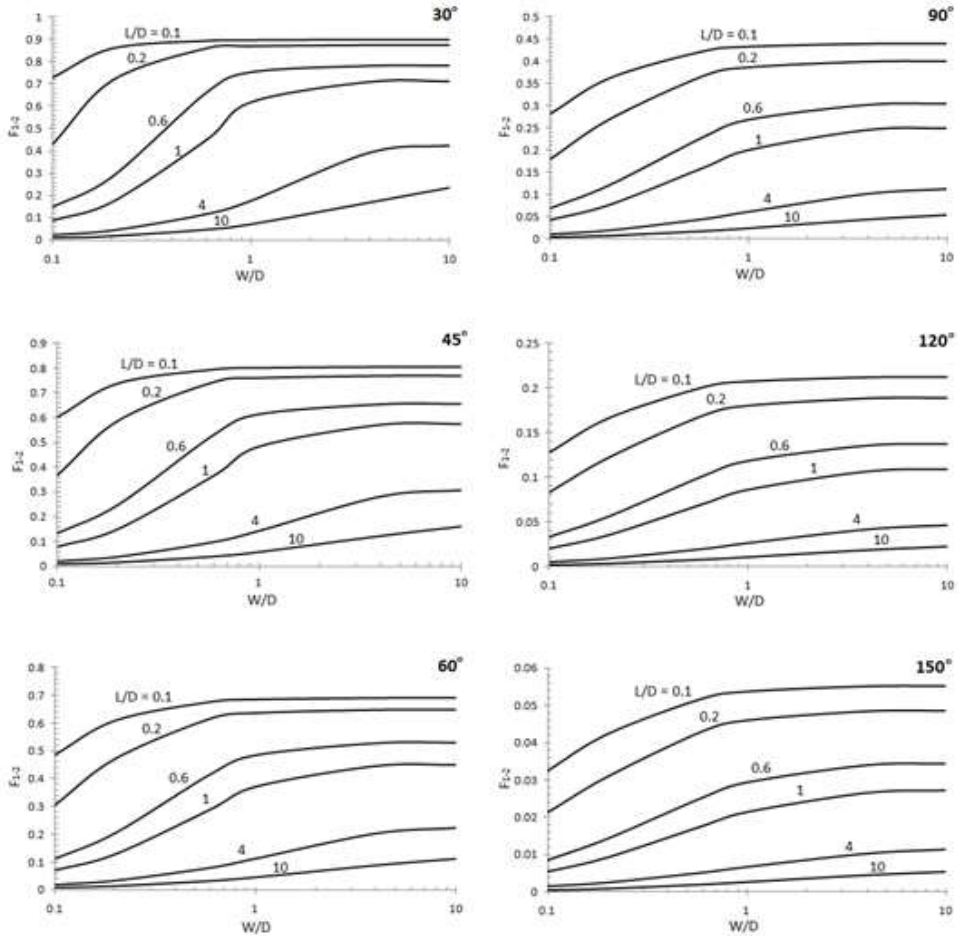

Figure 3. Values F_a-b obtained with Equation (4) for various θ values.

2.3. Generation of Triangular Meshes for Surface Elements

In modern engineering, mesh generators rarely use rectangles or squares unless the global geometry is a perfect cube. Triangular elements are among the most commonly used. The formulation of this type of geometry requires mathematical treatment involving several summations of the quadruple integral due to the variation of projection contours on the coordinate axes. Diagonal lines can be extended over the rectangular surfaces of Figure 2, subdividing the rectangular plane domain into triangular elements (Figure 4), for subsequent mesh generation and FEM implementation to determine view factors under complex boundary conditions.

In Figure 4, the emitting and receiving surfaces A_a and A_b are divided into four triangular surfaces, making $n^{n-1} = 4^{4-1} = 64$ =combinations possible. View factor reciprocity establishes that establece que $A_a F_{a-b} = A_b F_{b-a}$, for this reason, only 32 combinations will be evaluated. Figure 5 provides the basic geometries for cases 1 to 8, as these constitute the basis of the study, from

which the remaining combinations can be generated using summation rules. Figure 6 provides the basic geometries for cases 9 to 32.

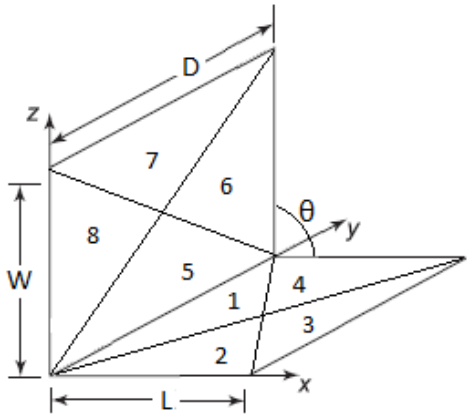

Figure 4. Decomposition of rectangular surfaces into triangular elements.

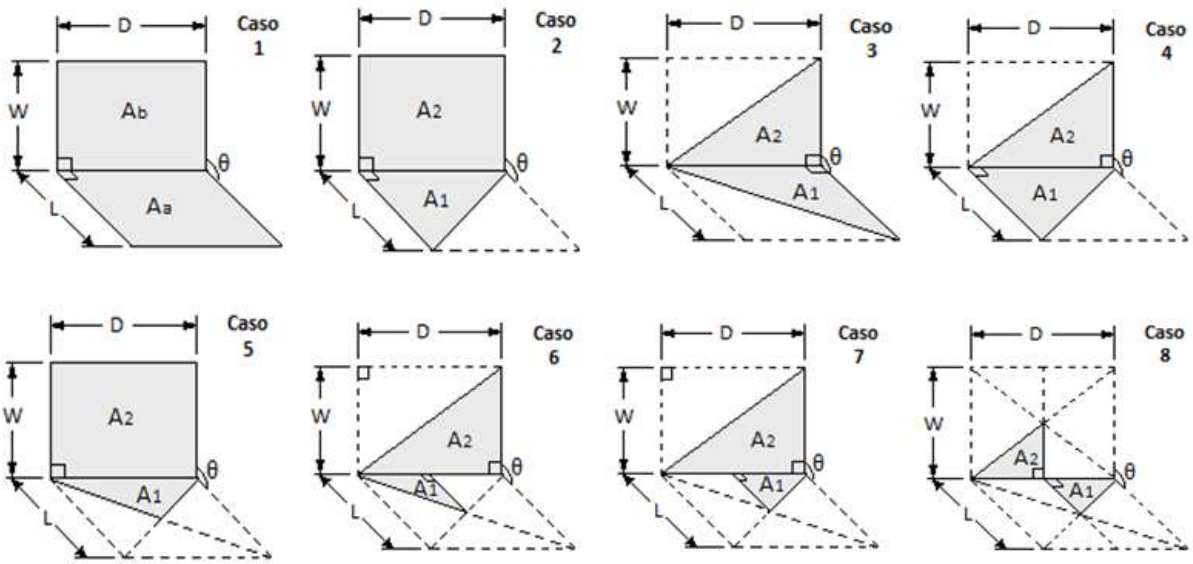

Figure 5. Basic view factor configurations for triangular surfaces (cases 1 to 8).

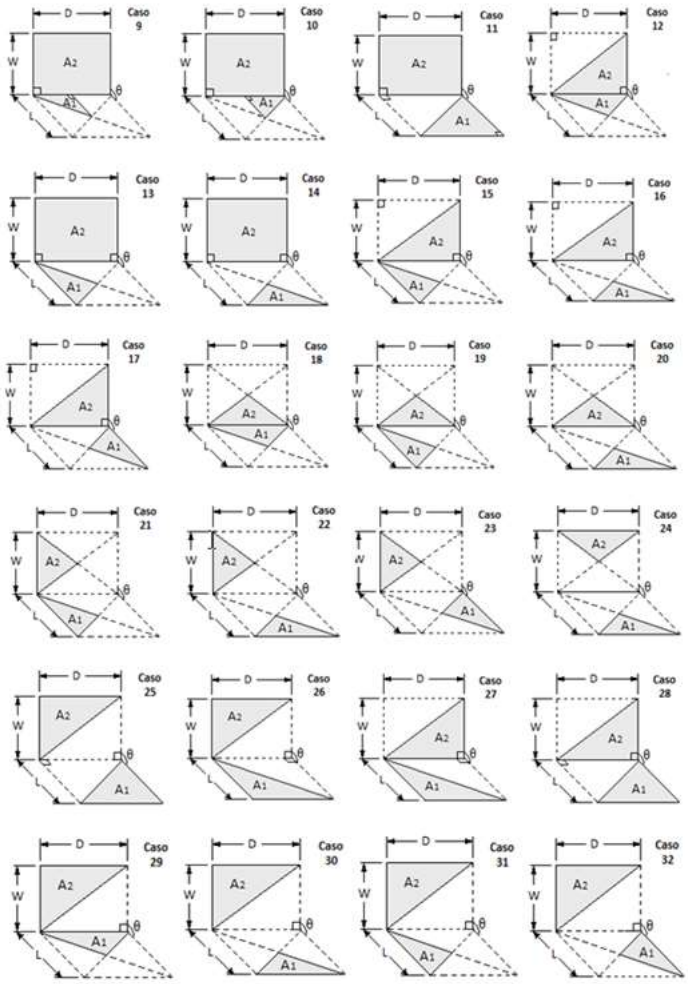

Figure 6. Derived view factor configurations for triangular surfaces (cases 9 to 32).

2.4. Mathematical Modeling of the View Factor

2.4.1. Case 2

In Case 2, the emitting and receiving surfaces are a rectangle and a right triangle, respectively, with a common side *D* and angle θ between both surfaces. In this Case (Figure 7), integration limits are established for each projection on surfaces A_1 and A_2, obtaining relationship (8):

$$f_{(2)} = F_{1-2} = \frac{1}{\pi A_1}\iint \frac{\cos O_1 \cos O_2 \, dA_1 dA_2}{r^2} =$$

$$\frac{\sin^2\theta}{\pi A_1}\int_0^L dy_1 \int_0^{y_1 D/L} dx \int_0^W dz \int_0^D \frac{xz}{\{(y_1-y_2)^2+x^2+z^2-2xz\cos\theta\}^2} dy_2 \qquad (8)$$

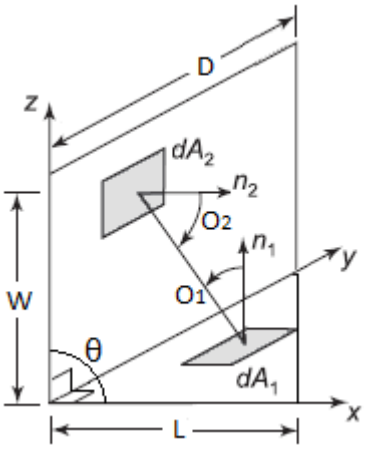

Figure 7. Basic geometry for Case 2

To execute the integration given in Equation (8), the following change of variables was performed (9):

$$W = a \;\; ; \;\; D = b \;\; ; \;\; L = c \tag{9}$$

The solution to Equation (8) is given by (10):

$$f_{(2)} = 2f_{(1)}\left\{\frac{a^2b^2}{8(a^2+b^2)}\ln\left(\frac{b^2+c^2}{(a^2+c^2)^2}\right)+\frac{a^2b^4}{4(a^2+b^2)^2}\ln\left(\frac{b(a^2+c^2)}{a(b^2+c^2)}\right)+\frac{a^4b^2}{4(a^2+b^2)^2}\ln\left(\frac{b}{a}\right)+\right.$$
$$\frac{a^2c^2}{8(a^2+b^2)}\ln\left(\frac{(b^2+c^2)(a^2+b^2+c^2)}{c^2(a^2+c^2)}\right)+\frac{a^2}{8}\ln\left(\frac{a^4(a^2+b^2+c^2)^2}{(a^2+b^2)^2(a^2+c^2)}\right)+\frac{b^2}{8}\ln\left(\frac{(a^2+b^2)(a^2+c^2)}{b^2(a^2+b^2+c^2)}\right)+$$
$$\frac{c^2}{8}\ln\left(\frac{c^2(a^2+b^2+c^2)}{(a^2+b^2)(a^2+c^2)}\right)+\frac{3}{4}ab\tan^{-1}\left(\frac{b}{a}\right)+\frac{1}{2}bc\tan^{-1}\left(\frac{b}{c}\right)-$$
$$\frac{1}{2}b\sqrt{a^2+c^2}\tan^{-1}\left(\frac{b}{\sqrt{a^2+c^2}}\right)-\frac{a^4}{8(a^2+b^2)}\ln(a^2+c^2)+\frac{ab^2(2a-\pi b)}{8(a^2+b^2)}+ \tag{10}$$
$$\frac{a^2b^2\left(\frac{b^4}{a^2+b^2}-b^2-c^2\right)}{2(a^2+b^2)^{\frac{3}{2}}\sqrt{b^2+c^2-\frac{b^4}{a^2+b^2}}}\tan^{-1}\left(\frac{(a^2+b^2)^{\frac{3}{2}}\sqrt{b^2+c^2-\frac{b^4}{a^2+b^2}}}{(a^2+b^2)^{\frac{3}{2}}\left(b^2+c^2-\frac{b^4}{a^2+b^2}\right)-b^2\{(a^2+b^2)-b^2\}}\right)-$$
$$\left.\frac{1}{2}\int_0^a\left[\frac{bx^2}{a\sqrt{x^2+c}}\tan^{-1}\left(\frac{a\sqrt{x^2+c}}{x^2+c^2+\frac{b^2}{a^2}(x^2-ax)}\right)+\frac{bx}{\sqrt{x^2+c}}\tan^{-1}\left(\frac{\frac{b}{a}x-b}{\sqrt{x^2+c}}\right)\right]dx\right\}$$

In Equation (10), the term $f_{(1)}$ is the view factor computed with Equation (4). Solving Equation (8) requires resolving $n^n = 4^4 = 256$ primitive functions; however, the final integral was not resolved as primitive functions do not exist for it, necessitating a solution via SMR (with seven intervals).

Obtaining an analytical solution for Equation (8) is extremely complex, as it involves the summation of infinite series with polylogarithms. An alternative solution is the complex variable treatment of these special functions, with the

addition of polynomials that progressively tend toward the convergence of the infinite Spence series, utilizing BCR.

Case 2 was obtained from the decomposition of rectangular surfaces into triangular elements (Figure 4); therefore, the solution of the quadruple integral of Equation (8) is derived from Equation (4) and can be expressed as in (11):

$$F_{1-2} = \varphi \cdot f_{(1)} \tag{11}$$

Where: $f_{(1)}$ is the view factor computed with Equation (4) and φ is the RCB.

The BCR is obtained from a stationary sum of view factors, fitting polynomials to the family of curves generated in the evaluated domain. There will be as many curves to fit as there are terms considered in the polylogarithmic series summation; thus, the increase in intervals will be proportional to the precision obtained in the results.

In Equation (4), it is observed that the view factor depends on two parameters (X, Y), with a common denominator D; therefore, the real root will be a function of these. The common side D is opposite to dimensions W, L on surfaces A_a y A_b, indicating that the period of the complex function (Camaraza-Medina, 2021) is given by (12):

$$\psi = \tan^{-1}\left(\frac{X}{Y}\right) \tag{12}$$

To apply the BCR, the solution of Equation (10) is graphically represented in the interval $0.1 \leq X \leq 10$ and $0.1 \leq Y \leq 10$ using values $X = Y = (0.1; 0.3; 0.6; 1; 3; 6; 10)$for its construction. Thus, from the upper and lower nodes, it is possible to draw the curve corresponding to the minimum and maximum values of $Y = (0.1; 10)$. In the infinite polylogarithmic series, a value of Y is fixed, and subsequently, the polylogarithms are calculated for each value of X; this procedure yields a family of curves a. Next, a similar procedure is applied, but fixing X values when calculating polylogarithms for each Y value, thus obtaining a family of curves b. Curves a y b are approximated individually using the least squares method, generating polynomials of the form $mX^3 + nX^2 + oX + p$. Constants m, n, o, p are subsequently weighted to generate a unique function φ, which depends on the formation angle φ (Camaraza-Medina, 2023).

Applying the method described in the previous paragraph, the BCR for Case 2 is given by (13):

$$\varphi_2 = (-0.022\mathrm{Y}^3 + 0.316\mathrm{Y}^2 - 0.89\mathrm{Y} + 0.5)\psi^2 +$$

$$(0.056\mathrm{Y}^3 - 0.783\mathrm{Y}^2 + 2.23\mathrm{Y} - 1.43)\psi - 0.03\mathrm{Y}^3 + 0.407\mathrm{Y}^2 - 1.07\mathrm{Y} + 2.02 \quad (13)$$

Substituting Equations (4) and (13) into Equation (11), the view factor for Case 2 is obtained via BCR, which is given by relationship (14):

$$f_{(2)} = F_{(1-2)} = \varphi_2 \cdot f_{(1)} \quad (14)$$

Figure (8) graphically presents the solution of Equation (14) for $\theta = 90°$.

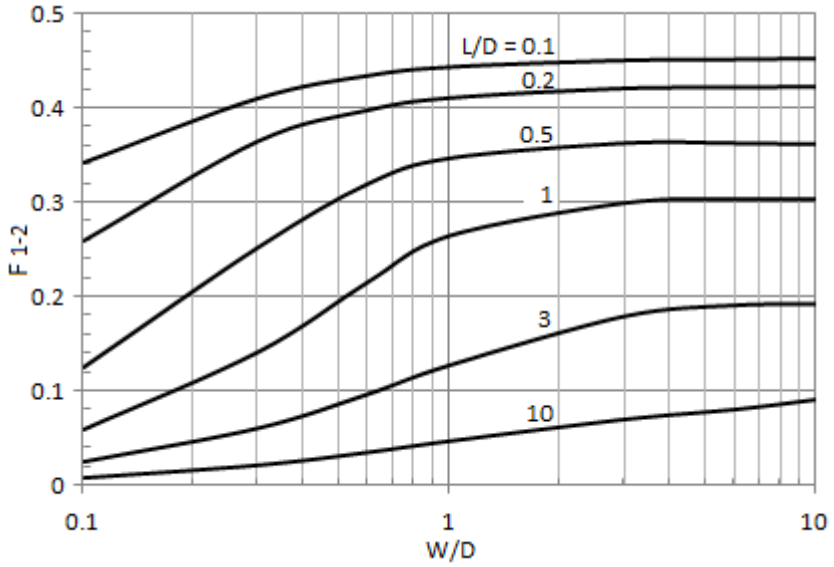

Figure 8. Graphical solution of Equation (14) for θ=90°

2.4.2 Cases 3 to 8

Cases 3 to 8 reduce to the following geometries (Figure 5):

- Case 3: Right triangle to right triangle, with common side and angle θ between both surfaces: vertices at a common point.
- Case 4: Right triangle to right triangle, with common side and angle θ between both surfaces: vertices at opposite ends.
- Case 5: Isosceles triangle to rectangle, with common side and angle θ between both surfaces.
- Case 6: Right triangle to right triangle of different sizes, with angle θ between both surfaces: vertices at a common point.
- Case 7: Right triangle to right triangle of different sizes, with angle θ between both surfaces: vertices at opposite ends.

- Case 8: Perpendicular right triangles with an equal edge and arranged in opposite directions.

In Cases 3 to 8 (Figure 5), integration limits are established for each projection on surfaces A_1 and A_2, obtaining integral relationships (15) to (20) as follows:

Case 3

$$f_{(3)} = \frac{\sin^2\theta}{\pi A_1}\int_0^L dy_1 \int_0^{y_1 D/L} dx \int_0^W dy_2 \int_0^{y_2 D/W} \frac{xz}{\{(y_1-y_2)^2+x^2+z^2-2xz\cos\theta\}^2}\,dz \quad (15)$$

Case 4

$$f_{(4)} = \frac{\sin^2\theta}{\pi A_1}\int_0^L dy_1 \int_0^{y_1 D/L} dx \int_0^W dy_2 \int_0^{y_2 D/W} \frac{xz}{\{(y_1-y_2)^2+x^2+z^2-2xz\cos\theta\}^2}\,dz \quad (16)$$

Case 5

$$f_{(5)} = \frac{\sin^2\theta}{\pi A_1}\int_0^{L/2} dy_1 \int_0^{y_1 D/L} dx \int_0^W dz \int_0^Z \frac{xz}{\{(y_1-y_2)^2+x^2+z^2-2xz\cos\theta\}^2}\,dy_2 \quad (17)$$

Case 6

$$f_{(6)} = \frac{\sin^2\theta}{\pi A_1}\int_0^{L/2} dy_1 \int_0^{y_1 D/L} dx \int_0^W dy_2 \int_0^{y_2 D/W} \frac{xz}{\{(y_1-y_2)^2+x^2+z^2-2xz\cos\theta\}^2}\,dz \quad (18)$$

Case 7

$$f_{(7)} = \frac{\sin^2\theta}{\pi A_1}\int_0^{L/2} dy_1 \int_{-y_1 D/L}^0 dx \int_0^W dy_2 \int_0^{y_2 D/W} \frac{xz}{\{(y_1-y_2)^2+x^2+z^2-2xz\cos\theta\}^2}\,dz \quad (19)$$

Case 8

$$f_{(8)} = \frac{\sin^2\theta}{\pi A_1}\int_0^{L/2} dy_1 \int_{-y_1 D/L}^0 dx \int_0^{W/2} dy_2 \int_0^{y_2 D/W} \frac{xz}{\{(y_1-y_2)^2+x^2+z^2-2xz\cos\theta\}^2}\,dz \quad (20)$$

While the BCR for each case are given by expressions (21) to (26):

Case 3

$$f_{(3)} = f_{(1)} \cdot \left\{ \begin{matrix} (-0.001\mathrm{Y}^3 + 0.033\mathrm{Y}^2 - 0.14\mathrm{Y} + 0.265)\psi^2 + \\ (0.011\mathrm{Y}^3 - 0.177\mathrm{Y}^2 + 0.7\mathrm{Y} - 0.615)\psi - 0.01\mathrm{Y}^3 + 0.142\mathrm{Y}^2 - 0.475\mathrm{Y} + 1.29 \end{matrix} \right\} \quad (21)$$

Case 4

$$f_{(4)} = f_{(1)} \cdot \left\{ \begin{matrix} (-0.031\mathrm{Y}^3 + 0.424\mathrm{Y}^2 - 1.275\mathrm{Y} + 1.1)\psi^2 + \\ (0.071\mathrm{Y}^3 - 0.975\mathrm{Y}^2 + 2.92\mathrm{Y} - 2.06)\psi - 0.034\mathrm{Y}^3 + 0.462\mathrm{Y}^2 - 1.268\mathrm{Y} + 1.6 \end{matrix} \right\} \quad (22)$$

Case 5

$$f_{(5)} = f_{(1)} \cdot \left\{ \begin{matrix} (-0.01\mathrm{Y}^2 + 0.24\mathrm{Y} + 0.67)\psi^2 + (0.02\mathrm{Y}^2 - 0.31\mathrm{Y} - 2.2)\psi - \\ 0.02\mathrm{Y}^2 + 0.27\mathrm{Y} + 3 \end{matrix} \right\} \quad (23)$$

Case 6

$$f_{(6)} = f_{(1)} \cdot \left\{ \begin{matrix} (-0.02\mathrm{Y}^3 + 0.29\mathrm{Y}^2 - 1.1\mathrm{Y} + 0.6)\psi^2 + (0.06\mathrm{Y}^3 - 0.88\mathrm{Y}^2 + 2.96\mathrm{Y} - 1.41)\psi - \\ 0.04\mathrm{Y}^3 + 0.55\mathrm{Y}^2 + +1.41\mathrm{Y} + 1.87 \end{matrix} \right\} \quad (24)$$

Case 7

$$f_{(7)} = f_{(1)} \cdot \left\{ \begin{matrix} (-0.011\mathrm{Y}^3 + 0.12\mathrm{Y}^2 - 0.025\mathrm{Y} + 0.52)\psi^2 + \\ (0.025\mathrm{Y}^3 - 0.307\mathrm{Y}^2 + 0.49\mathrm{Y} - 1.64)\psi - 0.014\mathrm{Y}^3 + 0.183\mathrm{Y}^2 - 0.35\mathrm{Y} + 2.47 \end{matrix} \right\} \quad (25)$$

Case 8

$$f_{(8)} = f_{(1)} \cdot \left\{ \begin{matrix} (0.015\mathrm{Y}^2 - 0.108\mathrm{Y} + 0.08)\psi^2 + (-0.015\mathrm{Y}^2 + 0.096\mathrm{Y} + 0.048)\psi - \\ 0.001\mathrm{Y}^2 + 0.04\mathrm{Y} + 0.058 \end{matrix} \right\} \quad (26)$$

Figure 9 graphically presents the solution of Equations (21) to (26), for $\theta = 90°$.

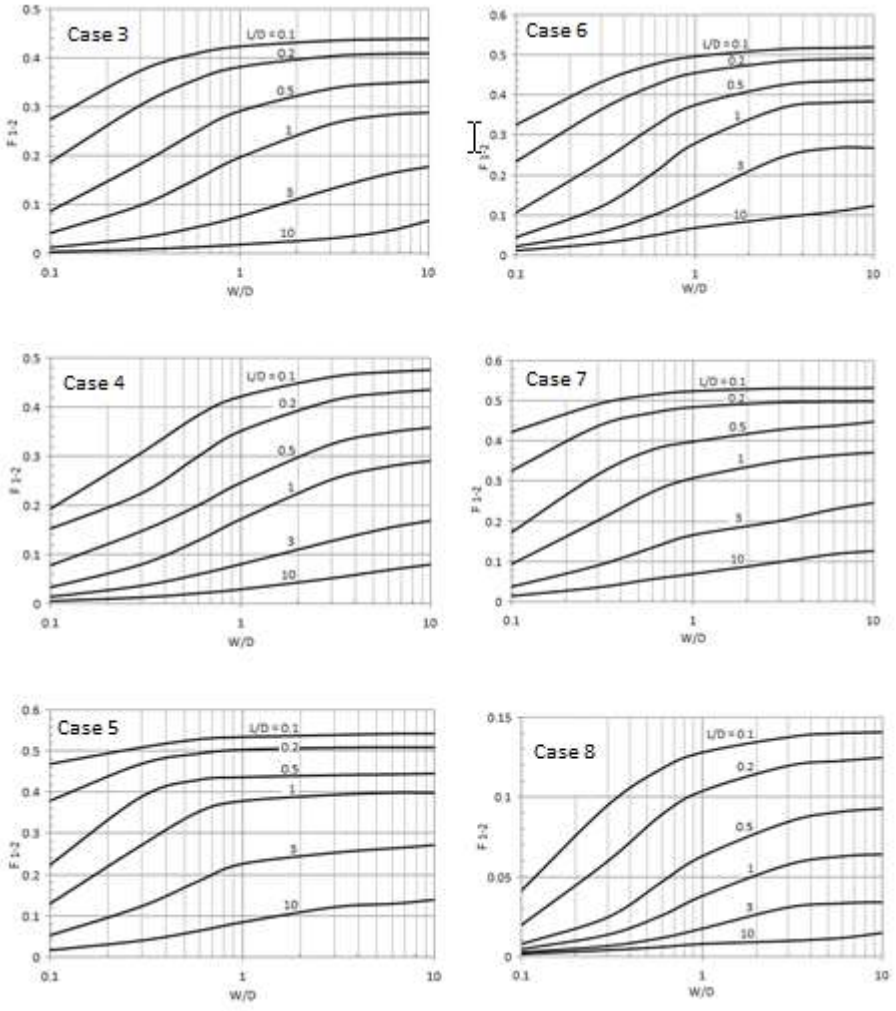

Figure 9. Graphical solution of Equations (21) to (26) for θ=90°

2.4.3. Cases 9 to 32

By combining view factors $f_{(1)}$ to $f_{(8)}$, it is possible to obtain the view factors for cases 9 to 32, applying summation rules and shape factor algebra. Table 2 summarizes the relationships for computing the view factor in the derived configurations (Figure 6, A and B).

Table 2. View factor configuration for triangular surfaces

Case	$\boldsymbol{F_{1-2}\cdots\{f_{(n)}\}}$
Case 9	$f_{(9)} = f_{(5)}$
Case 10	$f_{(10)} = f_{(5)}$
Case 11	$f_{(11)} = 2f_{(1)} - f_{(2)}$
Case 12	$f_{(12)} = f_{(6)} + f_{(7)}$
Case 13	$f_{(13)} = 2f_{(2)} - f_{(5)}$
Case 14	$f_{(14)} = 4f_{(1)} + f_{(5)} - 4f_{(2)}$
Case 15	$f_{(15)} = 2f_{(4)} - f_{(6)} - f_{(7)}$
Case 16	$f_{(16)} = 4f_{(1)} + f_{(6)} + f_{(7)} - 2f_{(3)} - 2f_{(4)}$
Case 17	$f_{(17)} = 2f_{(3)} - f_{(6)} - f_{(7)}$
Case 18	$f_{(18)} = f_{(3)} + f_{(8)}$
Case 19	$f_{(19)} = f_{(6)} + f_{(7)} - f_{(3)} - f_{(8)}$
Case 20	$f_{(20)} = 4f_{(5)} + f_{(3)} + f_{(8)} - 2f_{(6)} - 2f_{(7)}$
Caso 21	$f_{(21)} = 3f_{(3)} + f_{(8)} - 2f_{(6)} - 2f_{(7)}$
Case 22	$f_{(22)} = 4f_{(1)} + 3f_{(6)} + 3f_{(7)} - 3f_{(3)} - 2f_{(4)} - 4f_{(5)} - f_{(8)}$
Case 23	$f_{(23)} = 4f_{(5)} + f_{(3)} + f_{(8)} - 2f_{(6)} - 2f_{(7)}$
Caso 24	$f_{(24)} = 5f_{(3)} + 4f_{(4)} + 5f_{(5)} + f_{(8)} - 4f_{(1)} - 4f_{(2)} - 4f_{(6)} - 4f_{(7)}$
Caso 25	$f_{(25)} = 2f_{(1)} + f_{(4)} - 2f_{(2)}$
Case 26	$f_{(26)} = 2f_{(1)} + f_{(3)} - 2f_{(2)}$
Case 27	$f_{(27)} = f_{(2)} - f_{(3)}$
Case 28	$f_{(28)} = f_{(2)} - f_{(4)}$
Case 29	$f_{(29)} = f_{(5)} - f_{(6)} - f_{(7)}$
Case 30	$f_{(30)} = 2f_{(3)} + 2f_{(4)} + f_{(5)} - 4f_{(2)} - f_{(6)} - f_{(7)}$
Case 31	$f_{(31)} = 2f_{(2)} + f_{(6)} + f_{(7)} - f_{(5)} - 2f_{(4)}$
Case 32	$f_{(32)} = 2f_{(2)} + +f_{(6)} + f_{(7)} - f_{(5)} - 2f_{(3)}$

3. ANALYSIS OF RESULTS

The percentage deviation (error) is calculated with respect to the AS and is computed as expressed in (27):

$$D_{\%} = 100 \cdot \left(\frac{SA - Val}{SA}\right) \quad (27)$$

Where: $D_{\%}$ is the percentage deviation, in %. SA is the view factor computed using the analytical solution. Val is the view factor obtained with other methods.

Table 3 summarizes a comparison between view factors for twelve arbitrary geometric configurations, obtained via AS, SMR (with five intervals), SGS, and BCR using Equation (14), as well as the $D_{\%}$ values obtained with Equation (27).

Table 3. Comparison of view factors and D% obtained for Case 2

Configuration	Evaluation method				$D_{\%}$		
	AS	**SMR**	**SGS**	**BCR**	**SMR**	**SGS**	**BCR**
$X = 0.3$; $Y = 0.2$	0,36432	0,36013	0,36	0,36398	1,15	1,19	0,09
$X = 0.3$; $Y = 0.5$	0,25129	0,25072	0,25	0,25191	0,23	0,51	-0,25
$X = 0.3$; $Y = 1$	0,14106	0,15113	0,15	0,14087	-2,89	-2,79	0,13
$X = 1$; $Y = 0.5$	0,34661	0,34988	0,35	0,34687	-0,94	-0,98	-0,08
$X = 1$; $Y = 1$	0,26544	0,25978	0,26	0,26508	2,13	2,05	0,14
$X = 0.6$; $Y = 1$	0,21533	0,21886	0,22	0,21599	-1,64	-2,17	-0,31
$X = 0.6$; $Y = 3$	0,09588	0,09915	0,1	0,09627	-3,41	-4,3	-0,41
$X = 3$; $Y = 3$	0,18015	0,17894	0,18	0,17985	0,67	0,08	0,17
$X = 0.6$; $Y = 10$	0,03598	0,03882	0,04	0,03546	-7,89	-11,17	1,45
$X = 1$; $Y = 10$	0,04688	0,04833	0,05	0,04709	-3,09	-6,66	-0,45
$X = 10$; $Y = 1$	0,30886	0,30411	0,3	0,30731	1,54	2,87	0,5
$X = 10$; $Y = 10$	0,08879	0,08916	0,09	0,09021	-0,42	-1,36	-1,6

Figure 10 plots, within error bands of $\pm 3\%$ and $\pm 6\%$, $D_{\%}$ values obtained with Equation (18) for 48 view factors in the interval $0.1 \leq X, Y \leq 100$, calculated with SMR and BCR for Case 2.

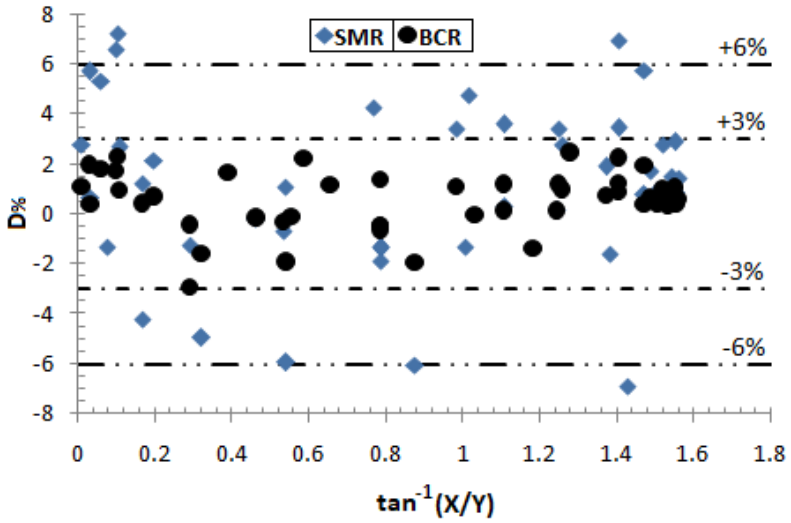

Figure 10. D% values obtained for Case 2.

For Case 2, Figure 10 shows that BCR provides a better fit with respect to the AS, with a mean error of $\pm 3\%$ in 100 % of the analyzed $(Y;X)$ points. Conversely, view factors obtained with SMR provide a lower fit with respect to the AS, with mean errors of $\pm 3\%$ y ± 6 and for 54.8% and 85.7% of the evaluated $(Y;X)$ points, respectively.

For Cases 3 to 8, Tables 4, 5, 6, 7, 8, and 9 summarize a comparison between view factors for twelve pre-established geometric configurations $(Y;X)$ obtained via AS, SMR (with five intervals), SGS solution, and BCR using Equations (21) to (26), as well as the $D_{\%}$ values obtained with Equation (27).

Table 4. Comparison of view factors and $D_{\%}$ obtained for Case 3

Configuration	Evaluation method				$D_{\%}$		
	AS	SMR	SGS	BCR	SMR	SGS	BCR
$X = 0.3\ ;\ Y = 0.2$	0,30198	0,30556	0,3	0,30353	-1,19	0,66	-0,51
$X = 0.3\ ;\ Y = 0.5$	0,18334	0,17885	0,18	0,18292	2,45	1,82	0,23
$X = 0.3\ ;\ Y = 1$	0,09776	0,1035	0,1	0,09847	-5,87	-2,29	-0,73
$X = 1\ ;\ Y = 0.5$	0,28983	0,28668	0,29	0,29087	1,09	-0,06	-0,36
$X = 1\ ;\ Y = 1$	0,19922	0,20092	0,2	0,19609	-0,85	-0,39	1,57
$X = 0.6\ ;\ Y = 1$	0,15402	0,15227	0,15	0,15316	1,14	2,61	0,56
$X = 0.6\ ;\ Y = 3$	0,05526	0,05876	0,06	0,05492	-6,33	-8,58	0,62
$X = 3\ ;\ Y = 3$	0,13119	0,12966	0,13	0,1313	1,17	0,91	-0,08
$X = 0.6\ ;\ Y = 10$	0,01361	0,01435	0,014	0,01327	-5,44	-2,87	2,5
$X = 1\ ;\ Y = 10$	0,01804	0,01896	0,02	0,01795	-5,1	-10,86	0,5

$X = 10\,;\, Y = 1$	0,28705	0,28106	0,28	0,28803	2,09	2,46	-0,34
$X = 10\,;\, Y = 10$	0,06884	0,06915	0,07	0,06665	-0,45	-1,69	3,18

Table 5. Comparison of view factors and $D_{\%}$ obtained for Case 4

Configuration	Evaluation method			$D_{\%}$			
	AS	SMR	SGS	AS	SMR	SGS	AS
$X = 0.3\,;\, Y = 0.2$	0,22553	0,22946	0,23	0,22471	-1,74	-1,98	0,36
$X = 0.3\,;\, Y = 0.5$	0,14683	0,14186	0,14	0,14769	3,38	4,65	-0,59
$X = 0.3\,;\, Y = 1$	0,08129	0,07966	0,08	0,08049	2,01	1,59	0,98
$X = 1\,;\, Y = 0.5$	0,24598	0,25148	0,25	0,24706	-2,24	-1,63	-0,44
$X = 1\,;\, Y = 1$	0,17409	0,17912	0,18	0,17202	-2,89	-3,39	1,19
$X = 0.6\,;\, Y = 1$	0,12881	0,12953	0,13	0,12908	-0,56	-0,92	-0,21
$X = 0.6\,;\, Y = 3$	0,06177	0,06098	0,06	0,06092	1,28	2,87	1,38
$X = 3\,;\, Y = 3$	0,12795	0,12916	0,13	0,12844	-0,95	-1,6	-0,38
$X = 0.6\,;\, Y = 10$	0,02063	0,02187	0,02	0,02117	-6,01	3,05	-2,62
$X = 1\,;\, Y = 10$	0,03048	0,03116	0,03	0,02976	-2,23	1,57	2,36
$X = 10\,;\, Y = 1$	0,29413	0,28776	0,29	0,29804	2,17	1,4	-1,33
$X = 10\,;\, Y = 10$	0,08054	0,08101	0,08	0,0808	-0,58	0,67	-0,32

Table 6. Comparison of view factors and $D_{\%}$ obtained for Case 5

Configuration	Evaluation method				$D_{\%}$		
	AS	SMR	SGS	BCR	SMR	SGS	BCR
$X = 0.3\,;\, Y = 0.2$	0,47668	0,46116	0,46	0,48334	3,26	3,5	-1,4
$X = 0.3\,;\, Y = 0.5$	0,39115	0,38942	0,39	0,39024	0,44	0,29	0,23
$X = 0.3\,;\, Y = 1$	0,27207	0,27085	0,27	0,27338	0,45	0,76	-0,48
$X = 1\,;\, Y = 0.5$	0,43765	0,43888	0,44	0,43666	-0,28	-0,54	0,23
$X = 1\,;\, Y = 1$	0,36884	0,36943	0,37	0,36998	-0,16	-0,31	-0,31
$X = 0.6\,;\, Y = 1$	0,35009	0,35073	0,35	0,34974	-0,18	0,03	0,1
$X = 0.6\,;\, Y = 3$	0,18415	0,18216	0,18	0,18602	1,08	2,25	-1,02
$X = 3\,;\, Y = 3$	0,25532	0,24991	0,25	0,2542	2,12	2,08	0,44
$X = 0.6\,;\, Y = 10$	0,06544	0,06888	0,07	0,06419	-5,26	-6,97	1,91
$X = 1\,;\, Y = 10$	0,08596	0,09012	0,09	0,08454	-4,84	-4,7	1,65
$X = 10\,;\, Y = 1$	0,39048	0,39777	0,4	0,38246	-1,87	-2,44	2,05
$X = 10\,;\, Y = 10$	0,13045	0,12876	0,13	0,13124	1,3	0,34	-0,61

Table 7. Comparison of view factors and $D_{\%}$ obtained for Case 6

Configuration	Evaluation method				$D_{\%}$		
	AS	SMR	SGS	BCR	SMR	SGS	BCR
$X = 0.3\ ;\ Y = 0.2$	0,36187	0,35228	0,35	0,36463	2,65	3,28	-0,76
$X = 0.3\ ;\ Y = 0.5$	0,23651	0,23913	0,24	0,23443	-1,11	-1,48	0,88
$X = 0.3\ ;\ Y = 1$	0,12506	0,12887	0,13	0,12227	-3,05	-3,95	2,23
$X = 1\ ;\ Y = 0.5$	0,37901	0,38077	0,38	0,37623	-0,46	-0,26	0,73
$X = 1\ ;\ Y = 1$	0,27998	0,27966	0,28	0,28035	0,11	-0,01	-0,13
$X = 0.6\ ;\ Y = 1$	0,21234	0,21793	0,22	0,20936	-2,63	-3,61	1,4
$X = 0.6\ ;\ Y = 3$	0,10095	0,10144	0,1	0,10305	-0,49	0,94	-2,08
$X = 3\ ;\ Y = 3$	0,24202	0,22308	0,22	0,24523	7,83	9,1	-1,33
$X = 0.6\ ;\ Y = 10$	0,05096	0,05063	0,05	0,05078	0,65	1,88	0,35
$X = 1\ ;\ Y = 10$	0,06734	0,06133	0,06	0,06916	8,92	10,9	-2,7
$X = 10\ ;\ Y = 1$	0,38714	0,38901	0,39	0,38532	-0,48	-0,74	0,47
$X = 10\ ;\ Y = 10$	0,11107	0,11233	0,11	0,11311	-1,13	0,96	-1,84

Table 8. Comparison of view factors and $D_{\%}$ obtained for Case 7

Configuration	Evaluation method				$D_{\%}$		
	AS	SMR	SGS	BCR	SMR	SGS	BCR
$X = 0.3\ ;\ Y = 0.2$	0,43944	0,43908	0,44	0,43825	0,08	-0,13	0,27
$X = 0.3\ ;\ Y = 0.5$	0,31644	0,31886	0,32	0,31778	-0,76	-1,13	-0,42
$X = 0.3\ ;\ Y = 1$	0,20644	0,20889	0,21	0,20212	-1,19	-1,72	2,09
$X = 1\ ;\ Y = 0.5$	0,40098	0,39976	0,4	0,40061	0,3	0,24	0,09
$X = 1\ ;\ Y = 1$	0,30841	0,30963	0,31	0,30744	-0,4	-0,52	0,31
$X = 0.6\ ;\ Y = 1$	0,27551	0,27785	0,28	0,27297	-0,85	-1,63	0,92
$X = 0.6\ ;\ Y = 3$	0,13882	0,13796	0,14	0,13755	0,62	-0,85	0,91
$X = 3\ ;\ Y = 3$	0,20332	0,20611	0,21	0,20109	-1,37	-3,29	1,1
$X = 0.6\ ;\ Y = 10$	0,05691	0,05823	0,06	0,05722	-2,32	-5,43	-0,54
$X = 1\ ;\ Y = 10$	0,07394	0,06882	0,07	0,07575	6,92	5,33	-2,45
$X = 10\ ;\ Y = 1$	0,37018	0,37096	0,37	0,3712	-0,21	0,05	-0,28
$X = 10\ ;\ Y = 10$	0,11863	0,11854	0,12	0,11759	0,08	-1,15	0,88

Table 9. Comparison of view factors and $D_{\%}$ obtained for Case 8

Configuration	Evaluation method				$D_{\%}$		
	AS	SMR	SGS	BCR	SMR	SGS	BCR
$X = 0.3\ ;\ Y = 0.2$	0,06034	0,05817	---	0,05975	3,6	---	0,98
$X = 0.3\ ;\ Y = 0.5$	0,02594	0,02712	---	0,02545	-4,55	---	1,89
$X = 0.3\ ;\ Y = 1$	0,01416	0,01542	0,015	0,01403	-6,78	-5,93	0,92
$X = 1\ ;\ Y = 0.5$	0,06288	0,06147	---	0,06326	2,24	---	-0,6
$X = 1\ ;\ Y = 1$	0,03831	0,03716	0,037	0,03807	3	3,42	0,63
$X = 0.6\ ;\ Y = 1$	0,02617	0,02417	0,024	0,02629	7,64	8,29	-0,46
$X = 0.6\ ;\ Y = 3$	0,01268	0,01335	0,013	0,01227	-5,28	-2,52	3,23
$X = 3\ ;\ Y = 3$	0,03154	0,03076	---	0,03121	2,47	---	1,05
$X = 0.6\ ;\ Y = 10$	0,00588	0,00536	0,005	0,00604	8,84	14,97	-2,72
$X = 1\ ;\ Y = 10$	0,00786	0,00714	0,007	0,00782	9,16	10,94	0,51
$X = 10\ ;\ Y = 1$	0,06394	0,06605	---	0,06446	-3,3	---	-0,81
$X = 10\ ;\ Y = 10$	0,01557	0,01431	---	0,01541	8,09	---	1,03

Figure 11 plots, within error bands of $\pm 3\%$ y $\pm 6\%$, the $D_{\%}$values obtained with Equation (27) for 48 view factors in the interval $0.1 \leq X, Y \leq 10$ calculated with SMR and BCR for Cases 3 to 8.

Figure 11 shows that BCR provides the best fit regarding the AS in all cases from 3 to 8, with different mean error percentages in the analyzed $(Y; X)$ points. In Case 3, the mean error is $\pm 3\%$ in 97.6% of the $(Y; X)$ points. In Cases 4, 5, and 6, a mean error of $\pm 3\%$ is observed in 92.9%, 90.5%, and 95.5%, respectively, and $\pm 6\%$ in 100% of the analyzed $(Y; X)$ points in these cases. Mean errors were $\pm 3\%$ in 100% of the $(Y; X)$points analyzed in Cases 7 and 8.

Likewise, Figure 11 reveals that, conversely, view factors obtained with SMR provide a lower fit regarding AS, computing mean errors $\pm 3\%$ in 28.5% of the evaluated $(Y; X)$ points in Case 3; 38.1% in Case 4; 21.4% in Case 5; 26.2% in Case 6; 31.0% in Case 7; and 23.8% in Case 8. As well as mean errors of $\pm 6\%$ in 64.3% (Case 3); 69.0% (Case 4); 61.9% (Case 5); 71.4% (Case 6); 81.0% (Case 7); and 73.8% (Case 8) of the analyzed $(Y; X)$ points in each referred case.

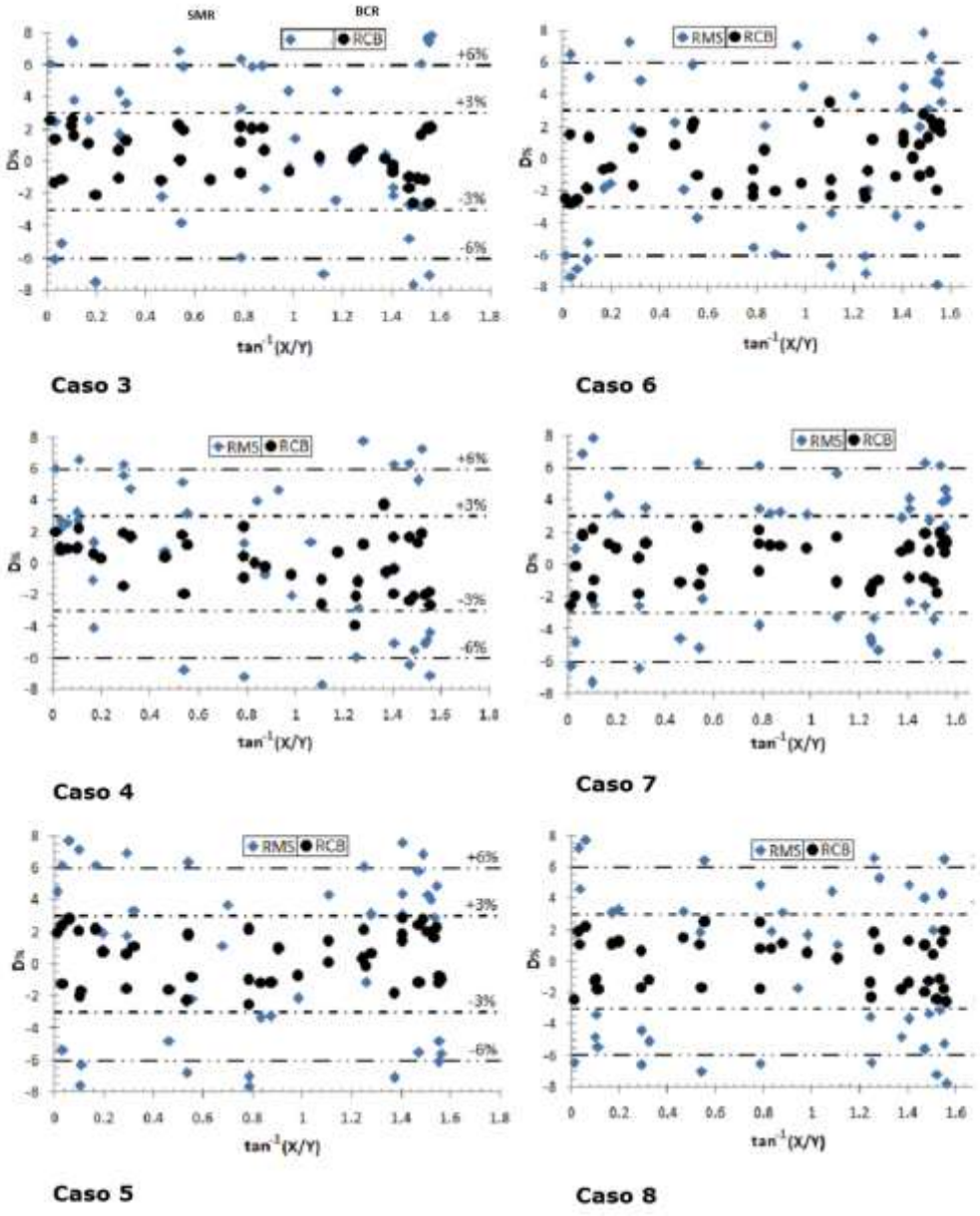

Figure 11. D% values obtained for Cases 3 to 8.

4. CONCLUSIONS

- Knowing the view factor is one of the most crucial aspects during radiant energy exchange, as an analytical solution considerably facilitates the work of thermal engineers, allowing for rapid and adequate estimation.

- This work provides information on the development of methods for view factor calculation during radiant energy exchange between 32 combinations of triangular geometries with a common edge.

- Twelve examples with various aspect ratios were calculated for each geometry, using AS, SMR, SGS, and BCR. From the eight basic geometries, the view factor for another 24 triangular geometries is obtained via summation rules. In all cases, identical fit values are achieved for SMR and SGS with respect to the AS, while the BCR shows the best fit in all examined cases.

- Given the practical nature of the contribution and the reasonable values of the fits obtained, the proposal constitutes a suitable tool for application in thermal engineering and related practices requiring thermal radiation calculations.

- Due to the lack of similar precedents in the literature, the proposed analytical solutions reinforce the scientific and practical value of this research and can be incorporated into currently available catalogs for view factor calculation.

5. REFERENCES

Biehs, S. A., Messina, R., Venkataram, P. S., Rodriguez, A. W., Cuevas, J. C. and Ben-Abdallah, P. (2021). Near-field radiative heat transfer in many-body systems. *Reviews of Modern Physics*, *93*(2), 025009.

Boeke, W. and Wall, L. (1976). Radiative exchange factors in rectangular spaces for the determination of mean radiant temperatures. *Building Services Engineer*, *43*, 244-253.

Bonnici, M., Mollicone, P., Fenech, M. and Azzopardi, M. A. (2019). Analytical and numerical models for thermal related design of a new pico-satellite. *Applied Thermal Engineering*, *159*, 113908.

Camaraza-Medina, Y., Hernandez-Guerrero, A., Luviano-Ortiz, J. L. (2022). Analytical view factor solution for radiant heat transfer between two arbitrary rectangular surfaces. *Journal of Thermal Analysis and Calorimetry*, *147*(24), 14999–15016.

Camaraza-Medina, Y. (2023). Aplicación de raíces cruzadas polinomiales al intercambio de energía radiante entre dos geometrías triangulares. *Ingenius, Revista de Ciencia y Tecnología*, *30*, 29-41.

Camaraza-Medina, Y. (2021). Methods for the determination of the heat transfer coefficient in air cooled condenser used at biomass power plants. *International Journal of Heat and Technology*, *39*(5), 1443-1450.

Camaraza-Medina, Y., Hernandez-Guerrero, A. and Luviano-Ortiz, J. L. (2023). View factor for radiative heat transfer calculations between triangular geometries with common edge. *Journal of Thermal Analysis and Calorimetry, 148*(10), 4523–4539.

DeSutter, J., Tang, L. and Francoeur, M. (2019). A near-field radiative heat transfer device. *Nature Nanotechnology*, *14*(8), 751-755.

Ehlert, J. R. and Smith, T. F. (1993). View factors for perpendicular and parallel rectangular plates. *Journal of Thermophysics and Heat Transfer*, *7*(1), 173-175.

Feingold, A. (1966). Radiant-interchange configuration factors between various selected plane surfaces. *Proceedings of the Royal Society of London*, *292*, 51-60.

Francisco, S. C., Raimundo, A. M., Gaspar, A. R., Oliveira, A. V. M. and Quintela, D. A. (2014). Calculation of view factors for complex geometries using Stokes' theorem. *Journal of Building Performance Simulation*, *7*(3), 203-216.

Gupta, M. K., Bumtariya, K. J., Shukla, H. A., Patel, P. and Khan, Z. (2017). Methods for evaluation of radiation view factor: a review. *Material Today Proceeding*, *4*(2), 1236-1243.

Hamilton, D. C. and Morgan, M. R. (1952). Radiant-interchange configuration factors. NASA TN 2836.

Howell, J. R. (2023). *A catalog of radiation heat transfer configuration factors* (7th ed.). MIT Press, United Kingdom, p. 180-185.

Howell, J. R. and Mengüç, M. P. (2011). Radiative transfer configuration factor catalog: A listing of relations for common geometries. *Journal of Quantitative Spectroscopy and Radiative Transfer*, *112*, 910-912.

Howell, J. R., Mengüç, J. P., Daun, K. and Siegel, R. (2020). *Thermal Radiation Heat Transfer* (7th ed.). CRC Press, USA, p. 105-106.

Krishnaprakas, C. K. (1997). View factor between inclined rectangles. *Journal of Thermophysics and Heat Transfer*, *11*(3), 480-481.

Lakhi, M. and Safavinejad, A. (2021). Numerical investigation of combined force convective–radiative heat transfer in a horizontal channel with lattice Boltzmann method. *Journal of Thermal Analysis and Calorimetry*, *146,* 1911-1922.

Modest, F. M. and Mazumder, S. (2021). *Radiative heat transfer* (4th ed.). Academic Press, United Kingdom, p. 130-145.

Narayanaswamy, A. (2015). An analytic expression for radiation view factor between two arbitrarily oriented planar polygons. *International Journal of Heat and Mass Transfer*, *91*, 841-847.

Narayanaswamy, A. and Meyappan, P. (2015). An analytic expression for radiation view factors between two planar triangles with arbitrary orientations. *Advances in Computational Heat Transfer*, *6*, 2015-2019

Nassar, Y. F. 2020. Analytical-numerical computation of view factor for several arrangements of two rectangular surfaces with non-common edge. *International Journal of Heat and Mass Transfer*, 159: 120130.

Reddy, R. S., Arepally, D. and Datta, A. K. (2023). View factor computation and radiation energy analysis in baking oven with obstructions: Analytical and numerical method. *Journal of Food Process Engineering*, *46*(3), 4270.

Sauer, H. J. (1974). Configuration factors for radiant energy interchange with triangular areas. *ASHRAE Transactions*, *80*(2), 268-279.

Sönmez, F. F., Ziar, H., Isabella, O. and Zeman, M. (2019). Fast and accurate ray-casting-based view factor estimation method for complex geometries. *Solar Energy Materials and Solar Cells*, *200*, 109934.

Thyageswaran, S. (2022). Simpler view factor calculations for mutually perpendicular rectangles. *Journal of Quantitative Spectroscopy and Radiative Transfer*, *283*, 108151.

Yarahmadi, M., Robert-Mahan, J. and McFall, K. (2020). Artificial neural networks in radiation heat transfer analysis. *ASME J Heat Transfer*, *142*(9), 092801.

Yi, X. J., Zhong, L. Y., Wang, T. B., Liu, W. X., Zhang, D. J., Yu, T. B. and Liu, N. H. (2019). Near-field radiative heat transfer between hyperbolic metasurfaces based on black phosphorus. *The European Physical Journal B.*, *92*, e217.

Zhou, Y., Duan, R., Zhu, X., Wu, J., Ma, J., Li, X. and Wang, Q. (2020). An improved model to calculate radiative heat transfer in hot combustion gases. *Combustion Theory and Modelling*, *24*(5), 829-851.

Additional Information

Conflict of Interest

There exist no conflict of interest

ORCID

YCM: https://orcid.org/0000-0003-2287-7519

Received: 01/03/2025
Accepted: 25/03/2025